Journal Name

ARTICLE

Vapochromic behaviour of a nickel(II)-quinonoid complex with dimensional changes between 1D and higher

Received 00th January 20xx,
Accepted 00th January 20xx

DOI: 10.1039/x0xx00000x

www.rsc.org/

Ryota Yano,[a] Masaki Yoshida,[a]* Takahiro Tsunenari,[a] Ayana Sato-Tomita,[b] Shunsuke Nozawa,[c] Youhei Iida,[d] Noriaki Matsunaga,[d] Atsushi Kobayashi [a] and Masako Kato [a]*

The nickel(II)-chloranilato complex $\{Ni(ca)(VM)_2\}_n$ (H_2ca = chloranilic acid, VM = coordinated vapour molecules, such as water) shows reversible vapochromism upon exposure to various vapours and subsequent drying by heating. In contrast to the Ni(II)-quinonoid complex, $[Ni(HL^{Me})]$ (H_2L^{Me} = 4-methylamino-6-methyliminio-3-oxocyclohexa-1,4-dien-1-olate), which was reported to exhibit vapochromic spin-state switching between high and low spin states, the chloranilato complex does not change its spin state even after the removal of coordinated vapour molecules. X-ray absorption fine structure (XAFS) analysis revealed that the six-coordinate geometry of $\{Ni(ca)(VM)_2\}_n$ was maintained even after the removal of vapour molecules, in contrast to the $[Ni(HL^{Me})]$ complex. The unique vapochromism that follows the dimensional change between 1D and higher is influenced by the relatively weaker ligand field of the chloranilate ligand.

Introduction

Vapochromism, a phenomenon of reversible colour changes induced by the adsorption and desorption of vapour molecules, has attracted considerable attention due to potential applications in the detection of harmful volatile organic compounds (VOCs).[1] To date, several vapochromic materials have been reported based on Pt(II) and Au(I) complexes. The vapochromic behaviours of these complexes are derived from a subtle change in the metal···metal interactions by the adsorption/desorption of vapour molecules, exhibiting remarkable colour and/or luminescence changes.[1] However, most previously reported vapochromic materials were focused only on colour changes. Multifunctional systems that exhibit changes in physical properties, such as magnetism and conductivity, coupled with colour changes, are still limited, although several vapochromic Fe(II)[2] and Co(II)[3] complexes capable of magnetic or spin switching have been reported.

We recently reported that a vapochromic Ni(II) complex bearing a quinonoid ligand, $[Ni(HL^{Me})_2]$ (H_2L^{Me} = 4-methylamino-6-methyliminio-3-oxocyclohexa-1,4-dien-1-olate)[4] (**1** in Scheme 1(a)) shows methanol-selective vapochromism coupled with spin-state switching.[5] This Ni(II) complex is remarkable in that it responds only to methanol vapour among various VOCs. On exposure of the crystalline purple powder of **1** to methanol vapour, a distinct colour change occurred, from purple to orange. X-ray crystallography of the methanol adduct (**1-MeOH**) revealed that methanol molecules were coordinated to the Ni(II) centre directly, forming an octahedral geometry. Concomitantly, **1-MeOH** exhibited a magnetic moment (3.07 μ_B), indicating the formation of a high-spin state of the Ni(II) complex, whereas the powder of **1** recovered by removing methanol molecules was diamagnetic, indicating the low-spin state of the Ni(II) complex. Ohkoshi and co-workers reported the crystalline-phase spin switching of a cyanido-bridged Ni(II)-W(IV) framework, $Ni_2[W(CN)_8]$, by water vapour.[6] Within this framework, the Ni(II) ions can adopt either anhydrous square-planar or water-coordinated octahedral geometries, leading to water vapour-driven vapochromism between the red diamagnetic state and the yellow-green paramagnetic state.

Thus, Ni(II)-complex systems are of particular interest for promising, multifunctional materials that exhibit magnetic properties controllable by vapour molecules, coupled with a colour change.[7] In fact, high-spin/low-spin equilibrium is well-studied for various Ni(II) complexes in solution,[8] and vapour-induced changes have also been achieved in a polymer film,[9] in a clay mineral,[10] or as an ionic liquid.[11] In the solid state, however, spin-state changes induced by vapour are still difficult to achieve,[12] although simple $Ni(CN)_2$ powder has been reported to show such reversible coordination-induced spin-state switching when immersed in water and subsequently dried via heating.[13] For the development of sophisticated, multifunctional systems with selectivity and sensitivity to vapour, it is necessary to explore the factors that control the crystal structures and their transformations.

[a] Department of Chemistry, Faculty of Science, Hokkaido University, North-10 West-8, Kita-ku, Sapporo, Hokkaido 060-0810, Japan. E-mail: myoshida@sci.hokudai.ac.jp, mkato@sci.hokudai.ac.jp
[b] Division of Biophysics, Department of Physiology, Jichi Medical University, 3311-1 Yakushiji, Shimotsuke, Tochigi 329-0498, Japan.
[c] Institute of Materials Structure Science, High Energy Accelerator Research Organization (KEK), 1-1 Oho, Tsukuba, Ibaraki 305-0801, Japan.
[d] Department of Physics, Faculty of Science, Hokkaido University, North-10 West-8, Kita-ku, Sapporo, Hokkaido 060-0810, Japan.

† Footnotes relating to the title and/or authors should appear here.
Electronic Supplementary Information (ESI) available: Vapour adsorption isotherm, PXRD patterns and diffuse reflectance spectra under vapour exposure, EXAFS spectra, theoretical data, and absorption spectra. See DOI: 10.1039/x0xx00000x

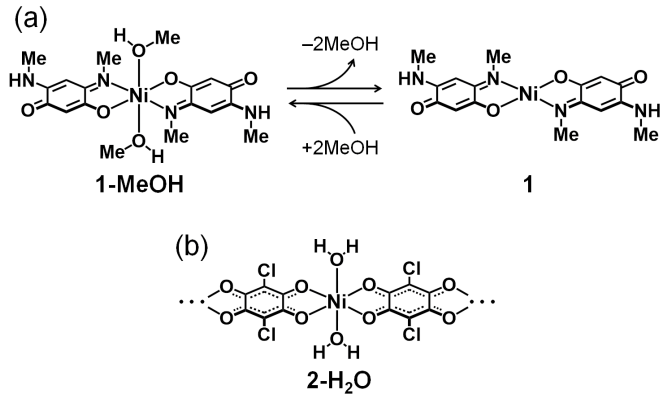

Scheme 1 (a) Structural formulas of **1-MeOH**, **1**, and (b) **2-H_2O**.

In this study, we investigated the vapochromic and magnetic behaviours of a Ni(II) complex bearing a chloranilate ligand, a different type of quinonoid ligand, $\{Ni(ca)(H_2O)_2\}_n \cdot 1.5nH_2O$ (**2-H_2O** in Scheme 1(b); H_2ca = chloranilic acid, n = degree of polymerisation). Although several metal-chloranilato complexes have been reported,[14] their chromic behaviours have not been studied. **2** exhibited a structural change accompanied by chromic phenomena under several vapours, including water, methanol, ethanol, acetonitrile, and THF. However, in contrast to **1**, a change in the spin state of **2** was not observed following vapour desorption. We then investigated the difference between the two systems. X-ray absorption fine structure (XAFS) analysis revealed that **2-H_2O** maintained its six-coordinate structure regardless of the coordination/desorption of water molecules, suggesting a unique, water molecule-induced structural transformation.

Experimental

Materials

Caution! *Although we experienced no difficulties, all the chemicals used in this study are potentially harmful and should be used in small quantities and handled with care in a fume hood.* $Ni(SO_4)\cdot 6H_2O$ and dibromomethane were purchased from FUJIFILM Wako Pure Chemical Co., Ltd. Chloranilic acid (H_2ca) was purchased from Sigma-Aldrich Co., Inc. All solvents were purchased from Kanto Chemical Co., Inc. All commercially available starting materials were used as received. **1-MeOH** was prepared according to the literature method.[5] All experiments were conducted under air.

Synthesis of $\{Ni(ca)(OH_2)_2\}_n \cdot 1.5nH_2O$ (2-H_2O). After H_2ca (523 mg, 2.5 mmol) was added to water (300 mL), the undissolved H_2ca was removed by filtration to prepare the saturated aqueous solution of H_2ca. A solution of $Ni(SO_4)\cdot 6H_2O$ (658 mg, 2.5 mmol) in water (100 mL) was added to the filtrate, and the mixture was stirred at room temperature for 20 h. The precipitate was collected by suction filtration and washed with water to yield a green solid. Yield: 670.6 mg (2.0 mmol, 80%). Anal. Calcd. for $C_6Cl_2NiO_4\cdot 3.5H_2O$: C, 21.92; H, 2.15. Found: C, 21.99; H, 1.85.

Measurements

UV-Vis absorption spectra and diffuse reflectance spectra were recorded on a Shimadzu UV-2500PC spectrophotometer. For UV-Vis diffuse reflectance spectroscopy, the solid samples were diluted by MgO, and the measured reflectivity was converted by the Kubelka-Munk function. Thermogravimetric analyses were conducted using a Rigaku Thermo plus EVO TG 8120 under Ar flow (0.3 L/min). Water vapour adsorption measurements were conducted using a MicrotracBEL BELSORP-max automatic volumetric adsorption apparatus. Magnetic susceptibility measurements were conducted using a Quantum Design MPMS3 magnetometer. Diamagnetic corrections were based on Pascal's constants.[15] IR spectra were recorded with a JASCO FT-IR 660 spectrometer equipped with a diamond attenuated total reflection (ATR) accessory. Elemental analyses were performed at the Analysis Centre of Hokkaido University.

Powder X-ray Diffraction

Powder X-ray diffraction (PXRD) measurements were conducted using Cu K_α radiation (λ = 1.5418 Å) on a Bruker D8 Advance diffractometer equipped with a graphite monochromator and a one-dimensional LynxEye detector using a non-reflective plate, or a Rigaku SPD diffractometer at the BL-8B beamline of the Photon Factory (PF), Japan. The synchrotron X-ray wavelength was 1.5455 Å. Lattice constants were refined for the experimental PXRD pattern by whole-powder-pattern decomposition (WPPD) method using the TOPAS 4 program.[16]

X-ray Absorption Fine Structure (XAFS) Analysis

Ni K-edge XAFS spectra were collected in the transmission mode at BL-9A beamline of the Photon Factory (PF), Japan. The incident X-ray was made monochromatic using a Si(111) double-crystal monochromator. The k^2-weighted EXAFS function, $k^2\chi(k)$, was extracted from the raw X-ray absorption data, which were obtained by using the ATHENA software.[17] A Fourier transform of the EXAFS function was conducted within the k range of 2–10 $Å^{-1}$ using a Hanning window.

Computational Methods

Geometry optimisations for **1**, $[Ni(Hca)_2]$ (**2'**; partial structure of **2**), and $[Ni(Hca)_2(H_2O)_2]$ (**2'-H_2O**; partial structure of **2-H_2O**) were performed without any constraint on the (U)M06L functional,[18] as implemented in the Gaussian09 program.[19] The SDD[20] basis set and its associated effective core potentials were applied for Ni, and the 6-311G**[21] basis set for other atoms. Vibrational frequency calculations confirmed that the optimised structures had no imaginary frequencies. Time-dependent density functional theory (TDDFT) was used for excited-state calculations, employing the UPBE1PBE functional[22] and the above basis sets. To obtain the simulated UV-vis absorption spectrum, transition energies and oscillator strengths have been interpolated by a Gaussian convolution with a common σ value of 0.333 eV. Cartesian coordinates for the optimised structures of complexes are summarised in Tables S1-S3. Calculated vertical excitations are summarised in Table S4.

Results and Discussion

Structure and Adsorption/Desorption Behaviour

The results of PXRD measurements of **2-H_2O** are shown in Fig. 1(a). The PXRD pattern showed qualitative agreement with the simulated pattern of the previously reported $\{Cu(ca)(OH_2)_2\}_n \cdot nH_2O$ (Fig. 1(a)),[23] indicating that **2-H_2O** is isostructural with $\{Cu(ca)(OH_2)_2\}_n \cdot nH_2O$. Therefore, similar to $\{Cu(ca)(OH_2)_2\}_n \cdot nH_2O$ (Fig. 1(b)), **2-H_2O** has a one-dimensional chain structure composed of Ni(II) ions and ca ligands along the *b* axis. In this structure, each Ni(II) ion adopted a six-coordinate octahedral geometry with ca ligands and 2 water molecules coordinated. The lattice constants of **2-H_2O** (Table 1) were obtained by optimising the PXRD pattern (Fig. S1) using the crystal parameters of $\{Cu(ca)(OH_2)_2\}_n \cdot nH_2O$. Among the lattice constants, the *a*- and *c*-axes of **2-H_2O** are elongated compared with those of $\{Cu(ca)(OH_2)_2\}_n \cdot nH_2O$ because of the large van der Waals radius of Ni (1.63 Å) compared with that of Cu (1.40 Å). In contrast, the *b*-axis of **2-H_2O** is shortened compared with that of $\{Cu(ca)(OH_2)_2\}_n \cdot nH_2O$ because of Jahn-Teller distortion in the Cu^{2+} ions (Scheme S1).

The vapour adsorption/desorption behaviour of **2-H_2O** was evaluated by thermogravimetric analysis and water vapour adsorption isotherm measurement. Thermogravimetric analysis of **2-H_2O** (Fig. 2) indicated two-step desorption behaviour: (i) a weight loss of 9.3 % (1.69 molecules of water) below 115 °C, and (ii) a weight loss of 10.2 % (2.09 molecules of water) from 115 to 200 °C. For the second weight loss, the differential thermal analysis (DTA) curve showed 2 endothermic peaks at 171 °C and 196 °C, corresponding to the stepwise removal of 2 coordinated water molecules. Therefore, **2-H_2O** initially releases 1.5 molecules of crystal water, and then 2 molecules of coordinated water to yield the anhydrous form **2** (Scheme 2). In addition, a large weight loss above 300 °C is assigned to the decomposition of the complex. To further confirm this behaviour, the water vapour adsorption isotherm of **2** was measured (Fig. S2). The rapid adsorption of 2.5 mol·mol^{-1} of water (per Ni) at relative humidity lower than 0.09 mainly corresponds to the chemisorption due to coordination to the Ni^{2+} ions. Subsequently, another molecule of water was adsorbed gradually until the relative humidity approached 1. This stepwise adsorption is in close agreement with the

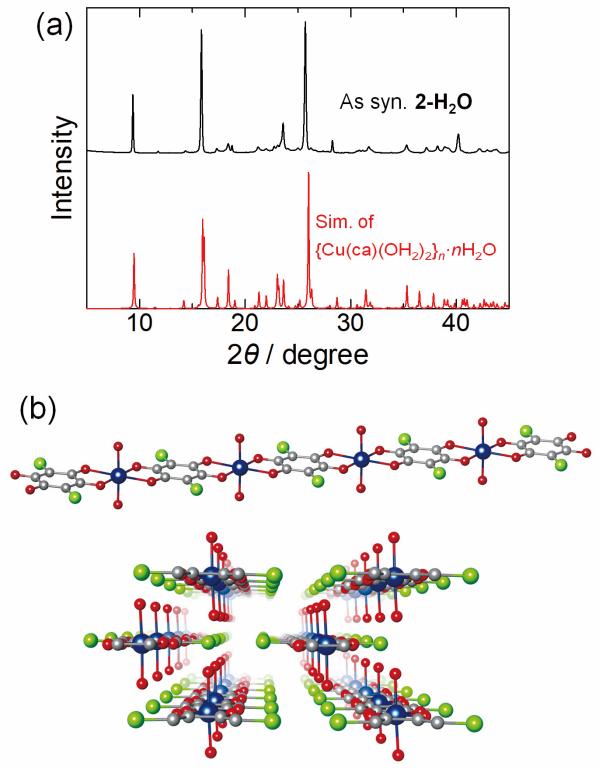

Fig. 1 (a) Powder X-ray diffraction pattern of **2-H_2O** and the simulated pattern based on the crystal structure of $\{Cu(ca)(OH_2)_2\}_n \cdot nH_2O$, an isostructural complex of **2-H_2O**, and (b) the crystal structure of the 1D arrangement (top) and the perspective view along the *b* axis (bottom) of $\{Cu(ca)(OH_2)_2\}_n \cdot nH_2O$ (grey: C, red: O, blue: Cu, green: Cl).[23] Crystal water molecules are omitted for clarity. The images were prepared using the VESTA program.[24]

Table 1. Lattice constants of $\{Cu(ca)(OH_2)_2\}_n \cdot nH_2O$[23] and **2-$H_2O$**, where the latter was estimated by the WPPD method.

	2-H_2O	$\{Cu(ca)(OH_2)_2\}_n \cdot nH_2O$
Formula	$C_6H_6Cl_2O_7Ni$	$C_6H_6Cl_2O_7Cu$
Temp. (K)	286	283-303
Crystal system	Triclinic	Triclinic
Space group	$P\bar{1}$	$P\bar{1}$
a (Å)	7.1299(8)	7.040(4)
b (Å)	7.8167(8)	7.962(4)
c (Å)	9.530(1)	9.364(5)
α (°)	84.71(1)	84.58(3)
β (°)	88.46(1)	89.25(3)
γ (°)	76.21(2)	76.53(3)
V (Å^3)	513.6(1)	508.1(5)
R_{wp} (%)	9.347	–
R, *wR* (%)	–	4.8, 5.0

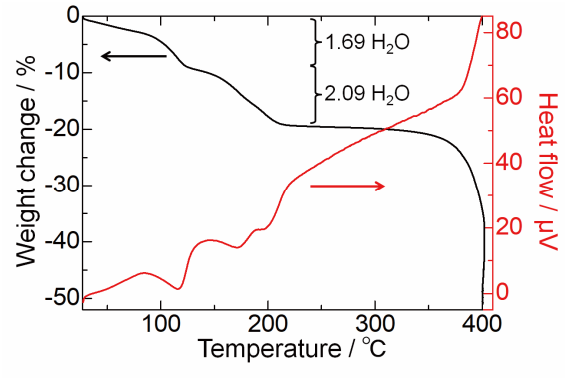

Fig. 2 Thermogravimetric analysis and differential thermal analysis of **2-H_2O**.

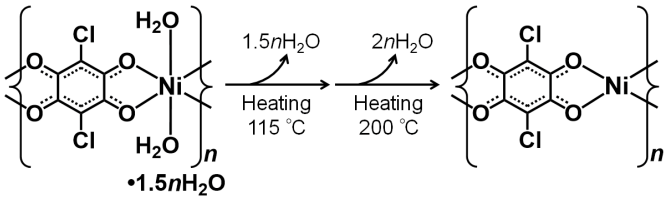

Scheme 2. The desorption of water molecules of **2-H_2O**.

thermogravimetric analysis result. In the desorption process, the desorption of only 1 molecule of water was observed, without further desorption of coordinated water molecules at 25 °C. This shows that heating at >200 °C is required for the desorption of the 2 coordinated water molecules of **2-H$_2$O**.

Vapochromic Behaviour

Fig. 3(a) shows the changes in the diffuse reflectance spectra of **2-H$_2$O** during the vapochromic response cycle. The as-synthesised powder of **2-H$_2$O** (black line in Fig. 3(a)) displayed an intense absorption band below 450 nm and a broad absorption band around 600 nm, resulting in a green colour. Interestingly, after the removal of water molecules by heating at 200 °C under Ar flow, the colour of the powder changed to dark brown due to the red-shift of the intense absorption band to ~500 nm (red line in Fig. 3(a)). The PXRD pattern changed significantly after drying (Fig. 3(b)), indicating a structural change. In addition, when this sample was exposed to water vapour at 45 °C, it returned to a dark-green powder, showing almost the same diffuse reflectance spectrum and PXRD pattern as the "As-syn." form. Therefore, we concluded that **2** exhibits a reversible vapochromism upon water vapour exposure.

In the next, anhydrous form **2** was exposed to methanol vapour or ethanol vapour for 50 h at 30 °C. Interestingly, after vapour exposure, distinct changes were observed in the PXRD patterns (orange and green lines in Fig. 3(b) for methanol and ethanol vapours, respectively), as well as the diffuse reflectance spectra (Fig. S3(a)). The PXRD patterns of the methanol- and ethanol-exposed samples were almost consistent with those of $\{Cu(ca)(MeOH)_2\}_n$[14b] and $\{Mn(ca)(EtOH)_2\}_n$[25] (Fig. S3(b-d)), respectively. Therefore, these methanol- and ethanol-exposed forms should adopt a six-coordinate octahedral structure in which 2 methanol or ethanol molecules are coordinated in the axial positions of the Ni(II) ion, i.e. $\{Ni(ca)(MeOH)_2\}_n$ and $\{Ni(ca)(EtOH)_2\}_n$. By heating these methanol- or ethanol-coordinated forms at 200 °C again, the anhydrous form **2** was restored (Fig. S4). In addition, when the anhydrous form **2** was exposed to methanol/water mixed vapour at 30 °C, the methanol-coordinated form was selectively obtained (Fig. S5), probably due to the difference in vapour pressure (4.2 kPa for water, 22 kPa for methanol, at 30 °C). We then evaluated the vapour response of **2** to several organic vapours under the same conditions. After exposure to MeCN vapour or tetrahydrofuran (THF) vapour, the PXRD patterns and diffuse reflectance spectra showed distinct changes from those of **2** (Fig. S6). On the other hand, when **2** was exposed to non-coordinating vapours, such as chloroform or dibromomethane, no change was observed in the PXRD patterns (Fig. S6(a)). These results suggest that the vapour-induced structural change of **2** is caused by the coordination of vapour molecules.

Magnetic Properties and XAFS Analyses

The magnetic properties of **2-H$_2$O** were investigated before and after the removal of the axial ligands (Fig. 4). The effective magnetic moment (μ_{eff}) of **2-H$_2$O** at 300 K was estimated to be 3.05 μ_B, indicating a typical high-spin Ni(II) ion

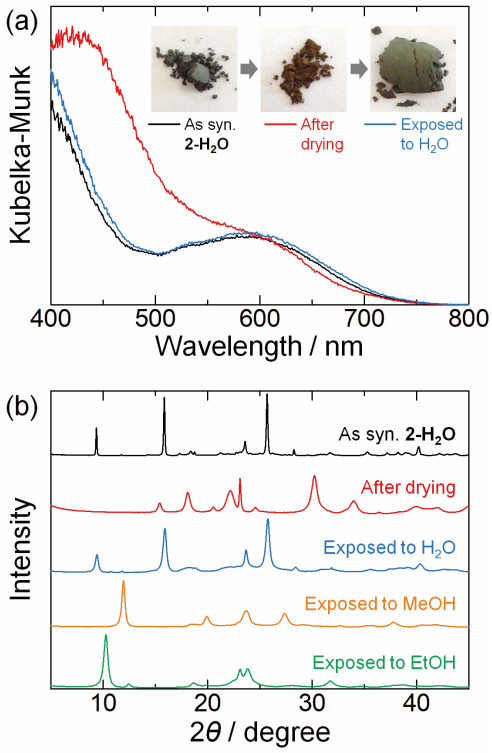

Fig. 3 Changes in the (a) diffuse reflectance spectrum and the (b) powder X-ray diffraction pattern of **2-H$_2$O** by heating and subsequent exposure to several vapours. Corresponding diffuse reflectance spectra of methanol- and ethanol-exposed forms were shown in Fig. S3(a). Inset photographs in (a) show images of **2-H$_2$O** during the vapochromic cycle.

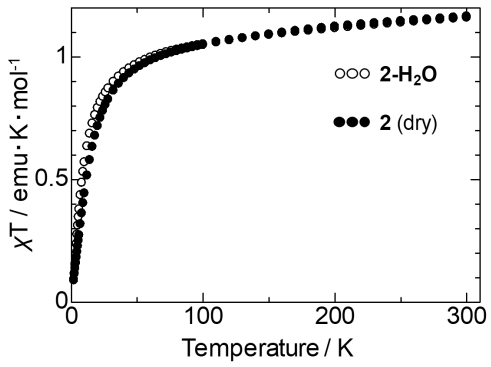

Fig. 4 Changes in the temperature-dependence of χT of **2-H$_2$O** at 10000 Oe upon the removal of water by heating at 250 °C under vacuum for 12 h.

with S = 1.[26] A small negative value of the Weiss temperature of **2-H$_2$O** (ϑ = -13.4 K) reveals a weak antiferromagnetic interaction between the Ni(II) ions *via* a one-dimensional chain. In contrast to **1**, which exhibited spin-state switching from S = 1 to S = 0 by the removal of the axial methanol ligands, the spin state of thepresent complex did not change even after desorption of coordinated vapour molecules by heating ($\mu_{eff(300\ K)}$ = 3.05 μ_B). The Weiss temperature changed slightly to -17.6 K after the desorption of water, indicating a slight enhancement of antiferromagnetic interactions.

To confirm the change in the local structure around the Ni(II) ion by vapour adsorption/desorption, X-ray absorption fine

structure (XAFS) measurements were performed on **2-H$_2$O** and anhydrous **2**. The k^2-weighted extended X-ray absorption fine structure (EXAFS) spectrum of the Ni-*K* edge and the corresponding Fourier transform are shown in Figs. S7 and 5(a), respectively. The broad peak at 1.53 Å is almost unchanged between these two forms, indicating that the Ni-O distance of **2-H$_2$O** did not change after the removal of the water ligands. On the other hand, for **1-MeOH**, the peak at 1.57 Å shifted significantly to 1.38 Å after the removal of the methanol ligands, indicating the shortening of bond distances after heating (Fig. 5(a)). This result is consistent with the change in the magnetic properties of **1-MeOH** after drying,[5] because the distance between Ni and the ligand should be shortened in the *S* = 0 spin state of the Ni(II) ion relative to the *S* = 1 state.[5,6] In the X-ray absorption near edge structure (XANES) region, both **2-H$_2$O** and **2** showed almost identical absorption edges (Fig. 5(b), top). Although **1-MeOH** also displayed a similar absorption edge, a shoulder peak appeared in the dried form **1** at ~8332 eV (Fig. 5(b), bottom). For square-planar four-coordinate Ni(II) complexes, dipole-allowed 1s → 4p$_z$ absorption was reportedly observed as a shoulder peak, owing to the destabilisation of the nearly-degenerated 4p$_x$ and 4p$_y$ orbitals relative to the 4p$_z$ orbital,[27] while such a shoulder peak was not observed for six-coordinate octahedral Ni(II) complexes. In addition, **1** also showed a pre-edge peak at 8328 eV, assigned to the 1s → 3d$_{x^2-y^2}$ absorption (Inset of Fig. 5(b)), indicating the unoccupied 3d$_{x^2-y^2}$ orbital in **1**. Therefore, the X-ray absorption spectra in both the XANES and the EXAFS regions revealed that **2-H$_2$O** maintained six-coordinate octahedral geometry with *S* = 1 spin state, even after the removal of the axial water ligands (**2**), in contrast to the geometrical change of **1-MeOH** from octahedral (*S* = 1) to square-planar (*S* = 0) by the removal of the methanol ligands. These results suggest that a large structural transformation occurred to maintain six-coordination after drying for **2**, with the axial positions of the Ni(II) ion occupied by the oxygen atoms of the ca ligands in the neighbouring one-dimensional chain (Scheme 3). A similar process has also been reported for the dehydration-induced trimerization of [Ni(acac)$_2$(H$_2$O)$_2$] (acac = acetylacetonate),[28] but the present system is unique because the structural change before and after desolvation is small compared to [Ni(acac)$_2$(H$_2$O)$_2$] to maintain the coordination polymer structure of **2**. Therefore, this is a unique vapochromism that allows a dimensional change between 1D and higher, although the X-ray crystal structure of the anhydrous form **2** has not yet been determined.

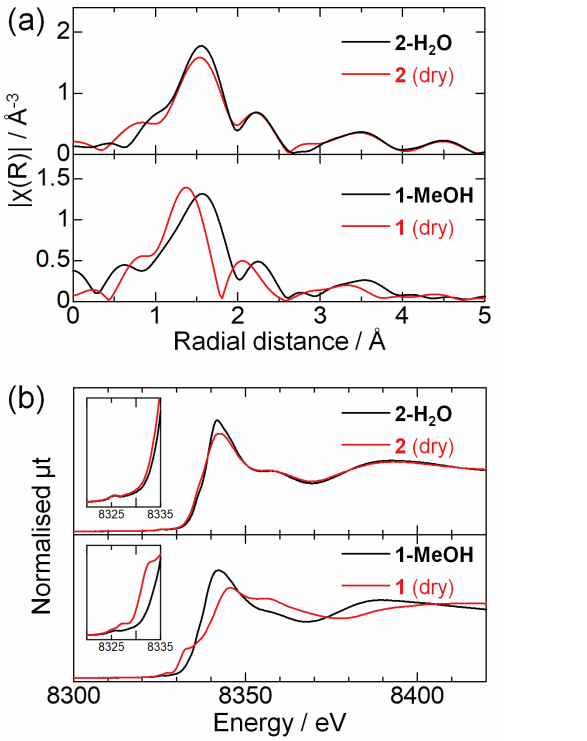

Fig. 5 Changes in (a) the EXAFS Fourier transform and (b) the XANES spectra of the Ni-*K* edge of **2-H$_2$O** and **1-MeOH** upon the removal of vapour molecules by heating at 250 °C under vacuum for 12 h. The corresponding EXAFS spectra are shown in Fig. S7. Insets in (b) show the magnification of the pre-edge region.

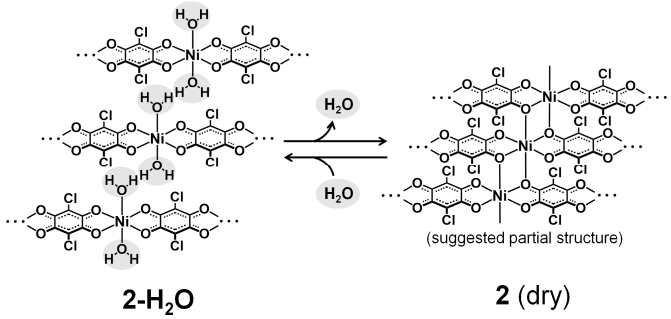

Scheme 3 Schematic illustration of the vapochromic behaviour of **2**.

Theoretical calculations

To gain better insight into the difference between **1** and **2**, we conducted density functional theory (DFT) calculations for **1** and [Ni(Hca)$_2$] (**2'**; partial structure of **2** with hypothetical square-planar geometry), as shown in Fig. 6. The Cartesian coordinates for the optimised ground state geometry are summarised in Tables S1-S2. The d_{z^2}–$d_{x^2-y^2}$ splitting of **2'** (1.914 eV) was significantly smaller than that of **1** (2.268 eV), indicating the relatively weak ligand-field strength of the chloranilate ligand compared with that of the HL^{Me} ligand. This result suggests that it is relatively difficult for **2'** to adopt the square-planar geometry compared with **1**. Therefore, **2** maintained the octahedral geometry, even after the removal of water ligands, by the coordination of the oxygen atoms in the neighbouring chain, in contrast to the geometrical and spin-state change of **1**.

We also attempted time-dependent DFT (TDDFT) calculations for the model compound **2'-H$_2$O** (Figs. S9-10) to address the origin of the vapochromism. The calculated key vertical excitation at λ_{calcd} = 642 nm (*f* = 0.0220) is in reasonable agreement with the experimental value (ca. 600 nm) for the lowest absorption band. According to the natural transition orbitals (NTOs), this absorption band was assigned to the intraligand $^1\pi\pi^*$ transition (Fig. S10). In addition, the intense absorption band below 450 nm was assignable to either the

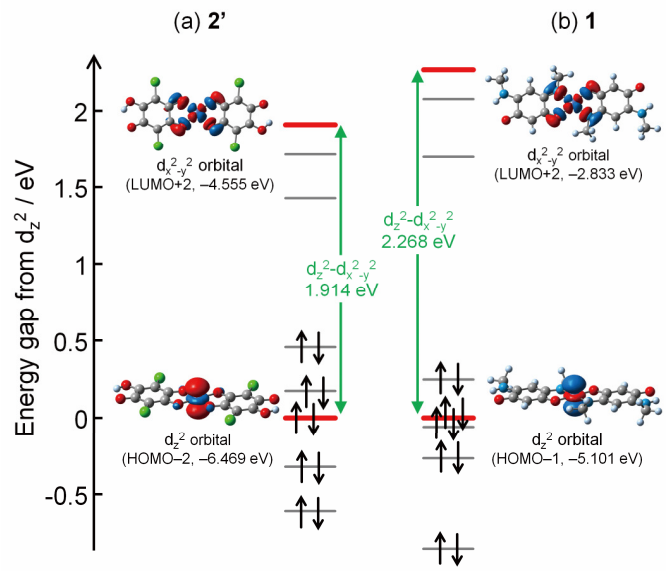

Fig. 6 Selected Kohn-Sham orbitals (isovalue = 0.035) and the energy level diagrams in the frontier region of optimised ground state structures of (a) **2'** and (b) **1**. The molecular orbitals in the frontier region are listed in Fig. S8.

$^1\pi\pi^*$ or $^1n\pi^*$ transitions of the chloranilate ligand (λ_{calcd} = 349 nm (f = 0.0137), λ_{calcd} = 343 nm (f = 0.2887), and λ_{calcd} = 327 nm (f = 0.1594); Fig. S10). Therefore, even though these absorption energies would not be directly perturbed by the removal of the vapour molecules on the Ni(II) ion, they should be affected by the environments around the ca ligands, such as π-stacking and/or the coordination mode of the ca ligands. Indeed, H_2ca showed a distinct absorption spectral change by deprotonation/protonation (Fig. S11),[29] indicating that the ca ligands should show environment-dependent absorption behaviour. As described in the previous section, the Ni(II) ion in the dry form **2** adopts the octahedral geometry, owing to the coordination of ca ligands from the neighbouring chains, which should increase the degree of π-stacking of the ca ligands and change of the coordination numbers of the O atoms, leading to a decrease in the $^1\pi\pi^*$ transition energy. Therefore, this would be one of the main origins of the vapochromism of **2-H_2O** without spin switching. This is supported by the fact that the vapochromic colour change of **2** was not very striking compared with that of **1**, which had a change in spin state.

Conclusions

We investigated the vapochromic behaviour of a new Ni(II)-quinonoid complex, **2-H_2O**. After the removal of the coordinated water molecules, **2** exhibited ligand-centred vapochromism in the presence of several vapours, including water, methanol, ethanol, acetonitrile, and THF. In contrast to the coordination/dissociation-induced spin-state switching behaviour of **1**, the spin state of **2** did not change even after the removal of the water molecules. Instead, a unique structural transformation followed by a dimensional change, from one-dimensional chains to a higher dimension, was revealed by XAFS analyses. The Ni(II) ion in **2-H_2O** maintained octahedral coordination geometry even after the removal of the water molecules, while **1-MeOH** exhibited a geometrical change from an octahedral to a square-planar geometry *via* the removal of the methanol molecules. Remarkably, the ligand field strongly influenced the vapochromic response of these Ni(II) systems. This study provides important information for the design of vapochromic Ni(II) complex systems to control spin-state switching coupled with a colour change.

Conflicts of interest

There are no conflicts of interest to declare.

Acknowledgements

This work was supported by JSPS KAKENHI grant numbers JP17H06367, JP17H06372, JP18K19086, and JP18K14232, and also by the Iketani Science and Technology Foundation. The PXRD and XAFS measurements were performed under the approval of the Photon Factory Programme Advisory Committee (Proposal No. 2019G511 and 2018S2-002, respectively). The supercomputing resources at the Research Centre for Computational Science, Okazaki, Japan are also acknowledged.

Notes and references

1 (a) M. Kato, *Bull. Chem. Soc. Jpn.*, 2007, **80**, 287–294; (b) O. S. Wenger, *Chem. Rev.*, 2013, 113, 3686–3733; (c) X. Zhang, B. Li, Z.-H. Chen and Z.-N. Chen, *J. Mater. Chem.*, 2012, **22**, 11427–11441; (d) A. Kobayashi and M. Kato, *Eur. J. Inorg. Chem.*, 2014, 4469–4483; (e) V. W.-W. Yam, V. K.-M. Au and S. Y.-L. Leung, *Chem. Rev.*, 2015, **115**, 7589–7728; (f) A. J. McConnell, C. S. Wood, P. P. Neelakandan and J. R. Nitschke, *Chem. Rev.*, 2015, **115**, 7729–7793.

2 (a) G. J. Halder, C. J. Kepert, B. Moubaraki, K. S. Murray and J. D. Cashion, *Science*, 2002, **298**, 1762–1765; (b) M. Ohba, K. Yoneda, G. Agustí, M. C. Munoz, A. B. Gaspar, J. A. Real, M. Yamasaki, H. Ando, Y. Nakao, S. Sakaki and S. Kitagawa, *Angew. Chem. Int. Ed.*, 2009, **48**, 4767–4771; (c) R.-J. Wei, J. Tao, R.-B. Huang and L.-S. Zheng, *Inorg. Chem.*, 2011, **50**, 8553–8564; (d) J. S. Costa, S. Rodríguez-Jimeńez, G. A. Craig, B. Barth, C. M. Beavers, S. J. Teat and G. Aromí, *J. Am. Chem. Soc.*, 2014, **136**, 3869–3874; (e) S. Rodríguez-Jiménez, H. L. C. Feltham and S. Brooker, *Angew. Chem. Int. Ed.*, 2016, **55**, 15067–15071.

3 (a) S. Ohkoshi, K. Arai, Y. Sato and K. Hashimoto, *Nat. Mater.*, 2004, **3**, 857–861; (b) S.-S. Bao, Y. Liao, Y.-H. Su, X. Liang, F.-C. Hu, Z. Sun, L.-M. Zheng, S. Wei, R. Alberto, Y.-Z. Li and J. Ma, *Angew. Chem. Int. Ed.*, 2011, **50**, 5504–5508; (c) P. Hu, L. Yin, A. Kirchon, J. Li, B. Li, Z. Wang, Z. Ouyang, T. Zhang and H.-c. Zhou, *Inorg. Chem.*, 2018, **57**, 7006–7014; (d) K. Komori-Orisaku, O. Stefańczyk, S. Ohishi, N. Ozaki, Y. Miyamoto, K. Imoto and S. Ohkoshi, *Chem. Eur. J.*, 2019, **25**, 11066–11073; (e) D. Shao, L. Shi, L. Yin, B.-L. Wang, Z.-X. Wang, Y.-Q. Zhang and X.-Y. Wang, *Chem. Sci.*, 2018, **9**, 7986–7991.

4 P. Braunstein, O. Siri, J.-p. Taquet, M.-M. Rohmer, M. Bénard and R. Welter, *J. Am. Chem. Soc.*, 2003, **125**, 12246–12256.

5 P. Kar, M. Yoshida, Y. Shigeta, A. Usui, A. Kobayashi, T. Minamidate, N. Matsunaga and M. Kato, *Angew. Chem. Int. Ed.*, 2017, **56**, 2345–2349.

6 M. Reczyński, S. Chorazy, B. Nowicka, B. Sieklucka and S. Ohkoshi, *Inorg. Chem.*, 2017, **56**, 179–185.

7 M. Kato, H. Ito, M. Hasegawa and K. Ishii, *Chem. Eur. J.*, 2019, **25**, 5105–5112.
8 (a) M. Sugimoto, M. Nonoyama, T. Ito and J. Fujita, *Inorg. Chem*., 1983, **22**, 950–954. (b) M. Dommaschk, V. Thoms, C. Schütt, C. Näther, R. Puttreddy, K. Rissanen and R. Herges, *Inorg. Chem.*, 2015, **54**, 9390–9392; (c) S. Thies, H. Sell, C. Bornholdt, C. Schütt, F. Kçhler, F. Tuczek and R. Herges, *Chem. Eur. J.*, 2012, **18**, 16358-16368; (d) S. Venkataramani, U. Jana, M. Dommaschk, F. D. Sönnichsen, F. Tuczek and R. Herges, *Science*, 2011, **331**, 445–448.
9 (a) A. Flamini, G. Mattei, A. Panusa, *J. Inclusion Phenom. Macrocyclic Chem.*, 1999, **33**, 377–390; (b) Y. Funasako and T. Mochida, *Chem. Commun.*, 2013, **49**, 4688–4690; (c) H. Hosokawa, Y. Funasako and T. Mochida, *Chem. Eur. J.*, 2014, **20**, 15014–15020.
10 H. Hosokawa and T. Mochida, *Langmuir*, 2015, **31**, 13048–13053.
11 Y. Funasako, T. Mochida, K. Takahashi, T. Sakurai and H. Ohta, *Chem. Eur. J.*, 2012, **18**, 11929–11936.
12 (a) E. Y. Lee and M. P. Suh, *Angew. Chem. Int. Ed.*, 2004, **43**, 2798–2801; (b) N. Baho and D. Zargarian, *Inorg. Chem.*, 2007, **46**, 299–308.
13 S. J. Hibble, A. M. Chippindale, A. H. Pohl and A. C. Hannon, *Angew. Chem. Int. Ed.*, 2007, **46**, 7116–7118.
14 (a) M. Verdaguer, A. Michalowicz, J. J. Girerd, N. Alberding and O. Kahn, *Inorg. Chem.*, 1980, **19**, 3271–3279; (b) S. Kawata, S. Kitagawa, M. Kondo, I Furuchi and M. Munakata, *Angew. Chem., Int. Ed.*, 1994, **33**, 1759–1761; (c) S. Kawata, S. Kitagawa, I. Furuchi, C. Kudo, H. Kamesaki, M. Kondo, M. Katada and M. Munakata, *Mol. Cryst. Liq. Cryst.*, 1995, **274**, 179–185.
15 O. Kahn, *Molecular Magnetism*, Willey-VCH, New York, 1993.
16 *TOPAS v4.2*, Bruker AXS, Karlsruhe, Germany, 2011.
17 B. Ravel and M. Newville, *J. Synchrotron. Rad.*, 2005, **12**, 537–541.
18 Y. Zhao and D. G. Truhlar, *J. Chem. Phys.*, 2006, **125**, 194101.
19 M. J. Frisch, G. W. Trucks, H. B. Schlegel, G. E. Scuseria, M. A. Robb, J. R. Cheeseman, G. Scalmani, V. Barone, B. Mennucci, G. A. Petersson, H. Nakatsuji, M. Caricato, X. Li, H. P. Hratchian, A. F. Izmaylov, J. Bloino, G. Zheng, J. L. Sonnenberg, M. Hada, M. Ehara, K. Toyota, R. Fukuda, J. Hasegawa, M. Ishida, T. Nakajima, Y. Honda, O. Kitao, H. Nakai, T. Vreven, J. A. Montgomery, Jr., J. E. Peralta, F. Ogliaro, M. Bearpark, J. J. Heyd, E. Brothers, K. N. Kudin, V. N. Staroverov, T. Keith, R. Kobayashi, J. Normand, K. Raghavachari, A. Rendell, J. C. Burant, S. S. Iyengar, J. Tomasi, M. Cossi, N. Rega, J. M. Millam, M. Klene, J. E. Knox, J. B. Cross, V. Bakken, C. Adamo, J. Jaramillo, R. Gomperts, R. E. Stratmann, O. Yazyev, A. J. Austin, R. Cammi, C. Pomelli, J. W. Ochterski, R. L. Martin, K. Morokuma, V. G. Zakrzewski, G. A. Voth, P. Salvador, J. J. Dannenberg, S. Dapprich, A. D. Daniels, O. Farkas, J. B. Foresman, J. V. Ortiz, J. Cioslowski and D. J. Fox, *Gaussian 09 (Revision E.01)*, Gaussian, Inc., Wallingford CT, 2013.
20 D. Andrae, U. Häussermann, M. Dolg, H. Stoll and H. Preuss, *Theor. Chim. Acta*, 1990, **77**, 123.
21 (a) R. Ditchfie, W. J. Hehre and J. A. Pople, *J. Chem. Phys.*, 1971, **54**, 724–728; (b) W. J. Hehre, R. Ditchfie and J. A. Pople, *J. Chem. Phys.*, 1972, **56**, 2257–2261; (c) P. C. Hariharan and J. A. Pople, *Theor Chim Acta*, 1973, **28**, 213-222; d) M. M. Francl, W. J. Pietro and W. J. Hehre, *J. Chem. Phys.*, 1982, **77**, 3654.
22 (a) M. Ernzerhof and G. E. Scuseria, *J. Chem. Phys.*, 1999, **110**, 5029–5036; (b) C. Adamo and V. Barone, *J. Chem. Phys.*, 1999, **110**, 6158–6170.
23 S. Cueto, H. P. Straumann, P. Rys, W. Petter, V. Gramlich and F. S. Rys, *Acta Cryst. C*, 1992, **48**, 458–460.
24 K. Momma and F. Izumi, *J. Appl. Cryst.*, 2011, **44**, 1272–1276.
25 S. Tanaka, A. Himegi, T. Ohishi, A. Fuyuhiro and S. Kawata, *Acta Cryst. E*, 2014, **70**, m90–m91.
26 C. E. Housecroft, A. G. Sharpe, *Inorganic Chemistry*, 3rd ed., Pearson Education, Harlow, 2008.
27 (a) M. K. Eidsness, R. J. Sullivan, J. R. Schwartz, P. L. Hartzell, R. S. Wolfe, A.-M. Flank, S. P. Cramer and R. A. Scott, *J. Am. Chem. Soc.*, 1986, **108**, 3120–3121; (b) L. R. Furenlid, M. W. Renner, D. J. Szalda and E. Fujita, *J. Am. Chem. Soc.*, 1991, **113**, 883–892; (c) M. P. Feth, A. Klein and H. Bertagnolli, *Eur. J. Inorg. Chem.*, 2003, 839–852; (d) X. Ottenwaelder, A. Aukauloo, Y. Journaux, R. Carrasco, J. Cano, B. Cervera, I. Castro, S. Curreli, M. C. Muñoz, A. L. Roselló, B. Soto and R. Ruiz-García, *Dalton Trans.*, 2005, 2516–2526.
28 (a) H. Montgomery and E. C. Lingafelter, *Acta Cryst.*, 1964, **17**, 1481–1482; (b) G. J. Bullen, R. Mason and P. Pauling, *Inorg. Chem.*, 1965, **4**, 456–462.
29 K. Molčanov and B. Kojić-Prodić, *CrystEngComm*, 2010, **12**, 925–939.